Upconversion Luminescence in Nanocrystals of Gd3Ga5O12 and Y3Al5O12 Doped with Tb3+−Yb3+ and Eu3+−Yb3+

ARTICLE *in* THE JOURNAL OF PHYSICAL CHEMISTRY C · JULY 2009

Impact Factor: 4.77 · DOI: 10.1021/jp901711g

6 AUTHORS, INCLUDING:

Stefano Polizzi
Università Ca' Foscari Venezia
141 PUBLICATIONS **3,272** CITATIONS
SEE PROFILE

Marco Bettinelli
University of Verona
514 PUBLICATIONS **9,285** CITATIONS
SEE PROFILE

Adolfo Speghini
University of Verona
321 PUBLICATIONS **6,708** CITATIONS
SEE PROFILE

Fabio Piccinelli
University of Verona
127 PUBLICATIONS **1,519** CITATIONS
SEE PROFILE

Upconversion Luminescence in Nanocrystals of $Gd_3Ga_5O_{12}$ and $Y_3Al_5O_{12}$ Doped with $Tb^{3+}-Yb^{3+}$ and $Eu^{3+}-Yb^{3+}$

R. Martín-Rodríguez,*,† R. Valiente,† S. Polizzi,‡ M. Bettinelli,§ A. Speghini,|| and F. Piccinelli§

Departamento de Física Aplicada, Universidad de Cantabria, 39005 Santander, Spain, Dipartimento di Chimica Fisica, Università di Venezia and INSTM, UdR Venezia, Via Torino 155/b, 30172 Venezia - Mestre, Italy, LabChimica dello Stato Solido, DB, Università di Verona and INSTM, UdR Verona, Ca' Vignal, Strada Le Grazie 15, I-37134 Verona, Italy, DiSTeMeV, Università di Verona and INSTM, UdR Verona, Villa Lebrecht - Via della Pieve, I-37029, San Floriano (Verona), Italy

Received: February 24, 2009; Revised Manuscript Received: April 23, 2009

$Gd_3Ga_5O_{12}$ and $Y_3Al_5O_{12}$ nanocrystalline powders codoped with Yb^{3+} and Tb^{3+} or Eu^{3+} have been prepared using the sol−gel Pechini method. Nanocrystals obtained by this technique exhibit a cubic phase with the $Ia\bar{3}d$ space group. Particles show a broad distribution of sizes and shapes, ranging from elongated to quasi-spherical particles of tens of nanometers. Optical properties such as photoluminescence and excitation spectra or lifetime measurements have been studied on these samples. Green/blue or red visible upconversion luminescence from Tb^{3+} $^5D_3$, $^5D_4 \rightarrow {}^7F_J$, or Eu^{3+} $^5D_0 \rightarrow {}^7F_J$ transitions, respectively, has been observed upon Yb^{3+} $^2F_{7/2} \rightarrow {}^2F_{5/2}$ excitation at 975 nm. A detailed investigation on the spectroscopy and excited state dynamics of these systems is extremely important in order to understand the upconversion processes.

1. Introduction

Upconversion (UC) is an interesting way to convert two or more low energy photons for obtaining higher energy emitted light from excited energy levels. At variance with two-photon absorption or second harmonic generation, real metastable intermediate energy levels are involved as reservoir storage for excitation energy, instead of a virtual state. The UC materials have attracted significant attention for advanced applications, such as solid state visible lasers, phosphor materials, optical data storage, IR counters, or in order to improve the efficiency of solar cells.[1−4] Very recently, Prasad and co-workers have used upconverting nanophosphors for photoluminescence bioimaging in vitro and in vivo providing deeper light penetration into the biological tissues, which are transparent in the 750−1000 nm range. The advantage of near-infrared (NIR) excitation is the reduction of the background autofluorescence of the tissues.[5] The vast majority of upconversion studies investigated to date have involved rare-earth ions. Due to the localized character of the f electrons the emission energies associated to f−f transitions are independent of the nanoparticle size. However, the emission intensity can be modified by the doping level or by the combination of rare-earth ions due to energy transfer processes.

It is well-known that Yb^{3+} is an excellent UC sensitizer for Er^{3+}, Tm^{3+}, Pr^{3+}, or Ho^{3+} ions.[6,7] The upconversion systems due to the codoping with these ions present the highest UC efficiencies. The UC processes involved in such systems can be ascribed to GSA/ETU (ground-state-absorption/energy-transfer-upconversion). All these ions present intermediate states almost resonant with the $^2F_{7/2} \leftrightarrow {}^2F_{5/2}$ Yb^{3+} transition. However, the situation is completely different for Tb^{3+} and Eu^{3+}, which have no intermediate levels resonant with Yb^{3+}. The ability of Yb^{3+} to induce UC is based on the high oscillator strength of the Yb^{3+} $^2F_{7/2} \rightarrow {}^2F_{5/2}$ transition, which is located in the NIR just in the range of inexpensive diode lasers (DL). Yb^{3+} has no higher excited states and it is transparent in the VIS region.

The Tb^{3+} and Eu^{3+} ions are attractive as emitting ions because of their high quantum efficiency related to the large energy gap between the emitting states and the low lying ^7F_J ($J = 0, 1, ..., 7$) excited states that, apart from Gd^{3+}, are the largest within lanthanides. Although the $Tb^{3+}-Yb^{3+}$ UC system was introduced in 1969,[8] only recently the potential application of this system as a quantum cutting phosphor via a cooperative downconversion mechanism has been shown.[9] On the contrary, as far as we know there are only few examples in the literature of UC luminescence in $Eu^{3+}-Yb^{3+}$ system.[10,11] $Gd_3Ga_5O_{12}$ (GGG) and $Y_3Al_5O_{12}$ (YAG) are materials suitable as hosts for luminescent lanthanide and transition metal ions. Taking into account the ionic radii, the impurity RE^{3+} ions are expected to replace Gd^3 and Y^{3+}.[12] This paper deals with the observation of visible Tb^{3+} and Eu^{3+} luminescence upon NIR excitation in $Tb^{3+}-Yb^{3+}$ and $Eu^{3+}-Yb^{3+}$ codoped nanocrystals of GGG and YAG. The UC luminescence is assigned, in both cases, to a cooperative sensitization mechanism.

2. Experimental Section

A. Synthesis and Structural Characterization. Nanocrystals of GGG and YAG codoped with nominal concentrations of $2\%Tb^{3+}-5\%Yb^{3+}$, $2\%Eu^{3+}-5\%Yb^{3+}$, and $2\%Eu^{3+}-1\%Er^{3+}$ were prepared by the sol−gel Pechini method[13] as described in ref 14. Briefly, the experimental procedure was as follows: the starting materials were reagent grade $Gd(NO_3)_3$, $Ga(NO_3)_3$, and $Ln(NO_3)_3$ for the GGG samples and $Y(NO_3)_3$, $Al(NO_3)_3$, and $Ln(NO_3)_3$ in the case of the YAG samples. Stoichiometric quantities of the starting reagents were dissolved in distilled water under stirring. Then the solution was heated at 90 °C and citric acid was added under stirring. Polyethylene glycol was then added to the solution, which was stirred for 15 min. The obtained sol was heated at 90 °C for 24 h in order to form the

* Correspondent author. E-mail: rosa.martin@unican.es.
† Universidad de Cantabria.
‡ Università di Venezia and INSTM.
§ LabChimica dello Stato Solido, DB, Università di Verona and INSTM.
|| DiSTeMeV, Università di Verona and INSTM.

10.1021/jp901711g CCC: $40.75
Published on Web 06/12/2009

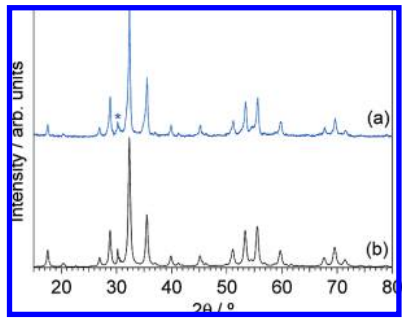

Figure 1. XRPD pattern of GGG: 2%Eu^{3+}, 5%Yb^{3+} prepared by the Pechini method (a) and the Rietveld fit (b). * indicates the main peak of the Gd_3GaO_6 impurity phase.

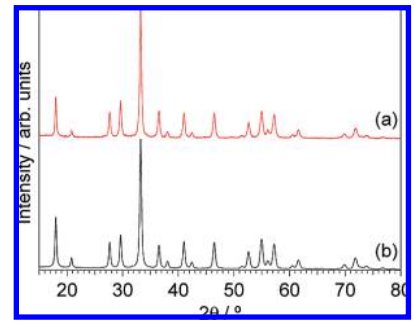

Figure 2. XRPD pattern of YAG: 2%Eu^{3+}, 5%Yb^{3+} prepared by the sol−gel Pechini method (a) and the Rietveld fit (b).

gel; finally, nanoparticles were obtained by firing this gel at 800 °C for 16 h.

X-ray measurements were used not only to check the phase purity of all samples but also to estimate the size of the obtained nanocrystallites. Diffraction patterns were collected using a Thermo Electron ARL X'TRA diffractometer equipped with a Cu-anode (Kα, $\lambda = 1.5418$ Å). The diffraction diagrams were recorded in a 2θ range of 5°−90° with a resolution of 0.03°/step and a scan rate of 0.8°/min. The MAUD program was used for Rietveld data refinement.[15] The X-ray fluorescence (ARL-XRF ADVANT'XP, Thermo) method was used to determine the average concentration of Tb^{3+}, Eu^{3+}, and Yb^{3+} in the nanocrystallites. The actual concentrations are consistent with the nominal ones taking into account the experimental uncertainty. Unfortunately, this technique cannot give us information about the impurity distribution within the nanoparticles.

Transmission electron microscopy (TEM) was performed on a JEOL 3010 operating at 300 kV equipped with a Gatan slow-scan 794 CCD camera. The sample powders were suspended in isopropanol and a 5 μL drop of this suspension was deposited on a holey carbon film supported on a standard 300 mesh copper grid.

B. Spectroscopy. Room temperature (RT) photoluminescence and excitation spectra of the title compounds were measured using a Fluorolog-2 spectrofluorometer (Jobin Yvon) exciting with a Xe lamp. The nanopowders were transferred into a quartz capillary and closed after partial evacuation. This allows us to measure all the samples in identical conditions. Continuous wave (CW) Tb^{3+} or Eu^{3+} upconversion luminescence spectra were obtained by exciting with a CW laser-diode (LD) emitting at 975 nm. The RT visible UC emission was detected with a Hamamatsu R928 photomultiplier. A fast InGaAs biased detector (Newport) was used for Yb^{3+} luminescence. All the spectra were taken under unfocused excitation and corrected for the system response. They are represented as photons counts vs wavenumbers. For fluorescence lifetime experiments, the 8−10 ns laser pulses of an OPO system (Vibrant II, Opotek) or modulated LD excitation were used. The sample luminescence was dispersed by a 0.50 m single monochromator (CHROMEX 500IS/SM) equipped with 500 nm blazed 1200 grooves/mm and 750 nm blazed 600 grooves/mm gratings, detected by a Hamamatsu (R928) photomultiplier or (R7102) extended IR photomultiplier and recorded with a multichannel scaler (Stanford Research SR-430).

3. Results

All of the prepared samples were analyzed using the X-ray powder diffraction (XRPD) technique. Figures 1 and 2 show the XRPD patterns of nanocrystalline GGG: 2%Eu^{3+}, 5%Yb^{3+} and YAG: 2%Eu^{3+}, 5%Yb^{3+} samples, respectively. The Rietveld refinement of the XRPD pattern of the GGG nanopowders (shown in Figure 1) is consistent with a cubic garnet single phase (space group $Ia3\bar{d}$, $a = 12.391$ Å) but contain small traces (up to 5%) of Gd_3GaO_6. The obtained lattice constant is similar to that found for an Eu^{3+} doped GGG nanocrystalline sample prepared by the same Pechini procedure.[16] Besides this, from Rietveld refinement, the average size of the crystallite grains was determined to be ca. 30 nm. The Eu^{3+}−Er^{3+} doped GGG samples are also single phase cubic garnet phase apart from a small trace contamination of Gd_3GaO_6 phase, as found for the Eu^{3+}−Yb^{3+} doped samples. Both the Eu^{3+}−Yb^{3+} and Eu^{3+}−Er^{3+} doped nanocrystalline YAG samples are composed of the cubic garnet phase ($Ia3\bar{d}$, $a = 12.031$ Å) without evidence of contamination from other phases. In Figure 2, the XRPD pattern of YAG: 2%Eu^{3+}, 5%Yb^{3+} is shown together with the Rietveld fit. The corresponding size of the crystallites obtained from Rietveld fitting is around 40 nm. There are no evidence of extra peaks due to phase segregation of the doping components.

TEM images of GGG and YAG samples (Figure 3) show that the samples are made of particles of different shapes and sizes, most of them in the range 20−80 nm. HRTEM images and the electron diffraction pattern (not shown) confirm the results of the XRPD analysis.

i. Tb^{3+}−Yb^{3+} System. Figure 4 compares the RT luminescence spectra of nanocrystalline GGG: 2%Tb^{3+}, 5%Yb^{3+} and YAG: 2%Tb^{3+}, 5%Yb^{3+} after visible and IR excitation. The first is obtained exciting directly the Tb^{3+} ions at 37 040 cm^{-1} (see below) while the UC luminescence is observed after the excitation of Yb^{3+} ions at 10 250 cm^{-1}. In all cases, the emission bands observed in the red-blue region (15 000−21 000 cm^{-1}) are assigned to the transitions from the $^5D_4$ multiplet to lower energy states ^7F_J of Tb^{3+} ions (Figure 5). Yb^{3+} pairs luminescence was not detected in our samples.

In addition to the f−f transitions plotted in the Dieke diagram, the excitation spectrum of YAG: 2%Tb^{3+}, 5%Yb^{3+}shows two intense bands at about 31 060 and 36100 cm^{-1}, which are assigned to f−d transitions.[17] Surprisingly, these bands were not detected in the case of GGG: 2%Tb^{3+}, 5%Yb^{3+} pointing out a different crystal field strength on the Tb^{3+} site. The excitation spectrum of Tb^{3+} in YAG (Figure 6a) consists of two strong bands, at 36 100 cm^{-1} and 31 060 cm^{-1}, with respect to the intensity of the f−f transitions. However, the high energy band is more than 1 order of magnitude stronger than the low energy one. We assign these transitions to the spin-allowed and spin-forbidden $4f-5d_t$ transitions of Tb^{3+}, in agreement with the data reported by Dorenbos for the same compound (36 500 and 30 860 cm^{-1}).[18] Excitation on the $4f-5d_t$ bands is followed by a fast nonradiative relaxation to the $^5D_3$ and $^5D_4$ multiplets, from where the emission takes place (Figure 6b).

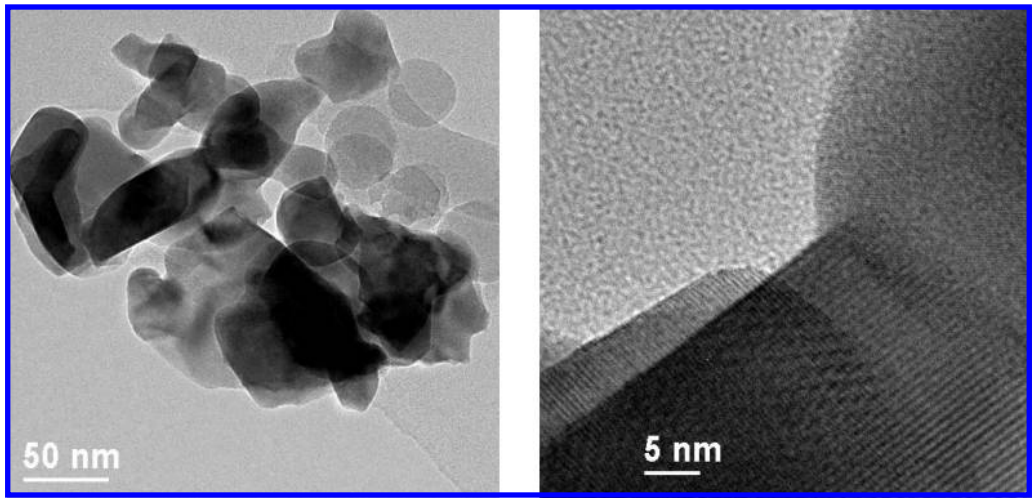

Figure 3. TEM images of GGG: 2%Tb^{3+}, 5%Yb^{3+} prepared by the sol−gel Pechini method. In the HRTEM image (right), the observed interplanar distances (0.298 nm) corresponds to the (012) crystal plane.

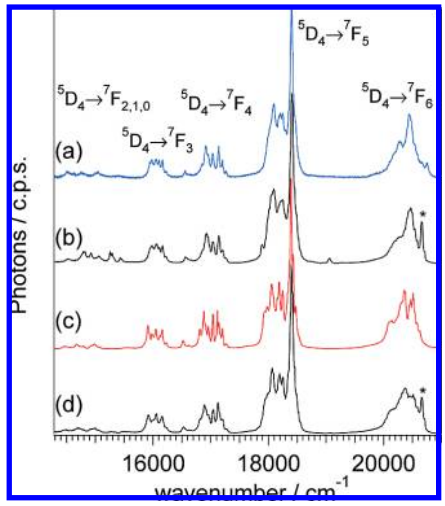

Figure 4. RT luminescence spectra of GGG: 2%Tb^{3+}, 5%Yb^{3+} exciting at 37 040 cm^{-1} (a) and 10 250 cm^{-1} (b). RT emission spectra of YAG: 2%Tb^{3+}, 5%Yb^{3+} exciting at 37040 cm^{-1} (c) and 10 250 cm^{-1} (d). * is an artifact and represents the laser at twice the excitation frequency.

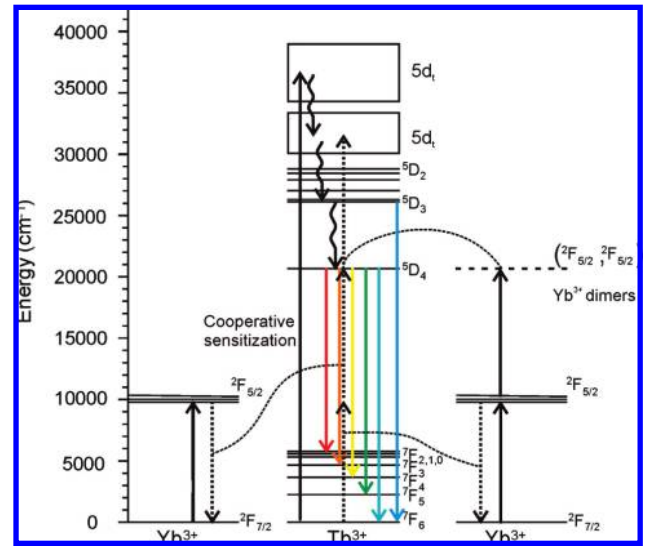

Figure 5. Energy level scheme of Tb^{3+} and Yb^{3+} ions with the $^5D_4 \rightarrow {}^7F_J$ and the $^5D_3 \rightarrow {}^7F_J$ Tb^{3+} luminescent transitions and the cooperative sensitization mechanism.

The presence of the parity allowed 4f−5d_t transitions in the near-UV region in the case of YAG: 2%Tb^{3+}, 5%Yb^{3+} makes this material suitable as a downconversion phosphor. Additionally, the demonstration of the Tb^{3+}−Yb^{3+} cooperative upconversion mechanism opens the possibility to use also this system as a downconversion phosphor, i.e. one Tb^{3+} ion would generate two Yb^{3+} ions in the excited state. This could be applied for the improvement of solar cell efficiency. This is particularly important taking into account that the 4f−5d_t bands in YAG: 2%Tb^{3+}, 5%Yb^{3+} are located close to band gap of clear glasses usually used integrated in front of the solar cell panels as protectors.

Green $^5D_4 \rightarrow {}^7F_J$ Tb^{3+} UC luminescence has been widely investigated, however, there are only few examples of blue UC Tb^{3+} emission from the $^5D_3$ multiplet in the literature. Luminescence from this state between 22 000 and 27 000 cm^{-1} was observed after IR excitation of YAG: 2%Tb^{3+}, 5%Yb^{3+} (Figure 6c). The only manner to access to the $^5D_3$ multiplet is via a three photon process (Figure 5). In order to prove this assumption we have measured the power dependence of the emitted photons of the $^5D_4 \rightarrow {}^7F_J$ and $^5D_3 \rightarrow {}^7F_J$ Tb^{3+} transitions upon IR excitation (Figure 7). Slopes of 2.6 and 3.3 are obtained for $^5D_4 \rightarrow {}^7F_J$ and $^5D_3 \rightarrow {}^7F_J$ Tb^{3+} emissions, respectively. With this result we can propose that a three photon process is also involved in the green $^5D_4 \rightarrow {}^7F_J$ luminescence, indicating the relevance of a nonradiative relaxation from the $^5D_3$ to $^5D_4$ states. Such a three photon process for the green UC Tb^{3+} emission has been previously observed.[19] This is in agreement with a possible cross-relaxation populating the $^5D_4$ from the $^5D_3$ state.[20]

ii. Eu^{3+}−Yb^{3+} System. Figure 8 shows the Stokes and anti-Stokes luminescence spectra of nanocrystalline GGG: 2%Eu^{3+}, 5%Yb^{3+} and YAG: 2%Eu^{3+}, 5%Yb^{3+}. Eu^{3+} emission is obtained upon direct excitation at 25 450 cm^{-1}, whereas Eu^{3+} UC luminescence is detected after excitation of Yb^{3+} ions at 10 250 cm^{-1}. Unlike Yb^{3+} to Tb^{3+} UC luminescence, there are only few examples of Yb^{3+} to Eu^{3+} UC emission in the literature.[10,11,21] The bands observed in the spectra are assigned to $^5D_0 \rightarrow {}^7F_J$ Eu^{3+} transitions (Figure 9). In the UC luminescence spectra, in addition to the Eu^{3+} f−f transitions, emission bands in the 14 500−15 500 cm^{-1} range due to Er^{3+} impurities are detected. This fact has been also observed very recently by Tanner[21] even with starting materials with purity of 99.999%.

In order to understand if Er^{3+} impurities play any role in the Yb^{3+} to Eu^{3+} UC luminescence process, nanocrystalline samples

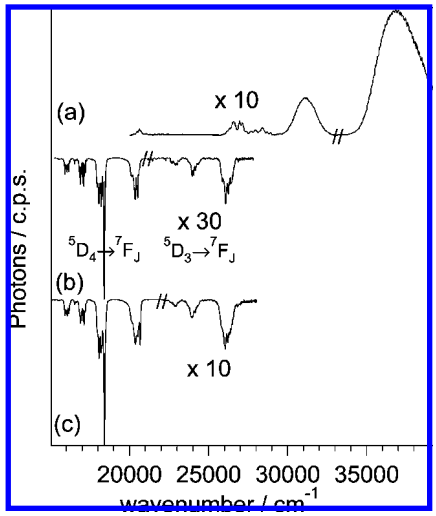

Figure 6. RT excitation spectrum of YAG: 2%Tb^{3+}, 5%Yb^{3+} (a), RT luminescence spectrum after excitation at 37 037 cm^{-1} (b), and RT emission spectrum after excitation at 10 250 cm^{-1} (c). Note the scale factors.

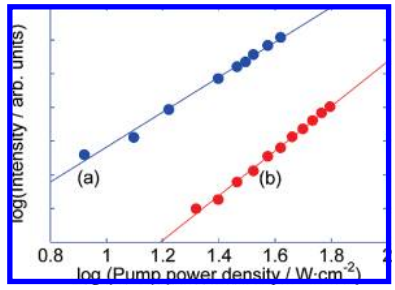

Figure 7. Excitation power dependence of the YAG: 2%Tb^{3+}, 5%Yb3+ 5D4 → 7FJ luminescence (a) and YAG: 2%Tb3+, 5%Yb3+ 5D3→7FJ emission (b) after10 250 cm−1 excitation.

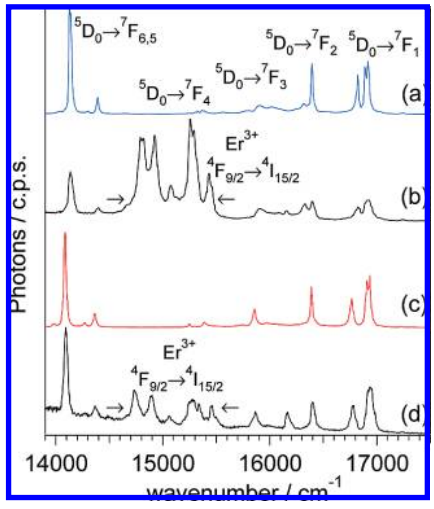

Figure 8. RT luminescence spectra of GGG: 2%Eu^{3+}, 5%Yb^{3+} exciting at 25 450 cm^{-1} (a) and 10 250 cm^{-1} (b). RT emission spectra of YAG: 2%Eu^{3+}, 5%Yb^{3+} exciting at 25 450 cm^{-1} (c) and 102 50 cm^{-1} (d). The emission corresponding to Er^{3+} transitions are shown between arrows.

of GGG: 2%Eu^{3+}, 1%Er^{3+} and YAG: 2%Eu^{3+}, 1%Er^{3+} were prepared and investigated. Figure 10 compares the UC luminescence of GGG: 2%Eu^{3+}, 1%Er^{3+} upon excitation of Er^{3+} ions with a LD at 10 250 cm^{-1} with that of GGG: 2%Eu^{3+}, 5%Yb^{3+} (Figure 10b). In Figure 10a, Er^{3+} excitation at 10 250 cm^{-1} is able to induce UC luminescence bands observed at

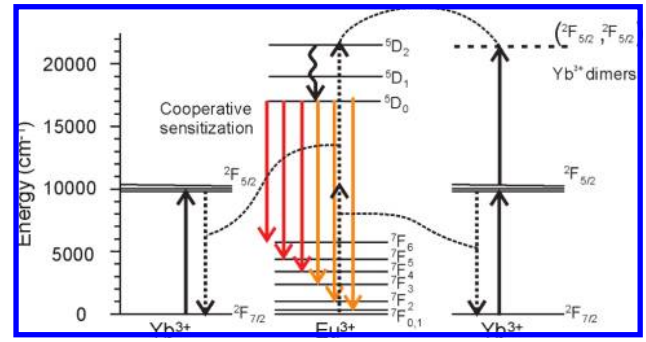

Figure 9. Energy level diagram of Eu^{3+} and Yb^{3+} ions with the $^5D_0 \rightarrow {}^7F_J$ Eu^{3+} emissions and the proposed $Yb^{3+}-Eu^{3+}$ energy transfer mechanisms.

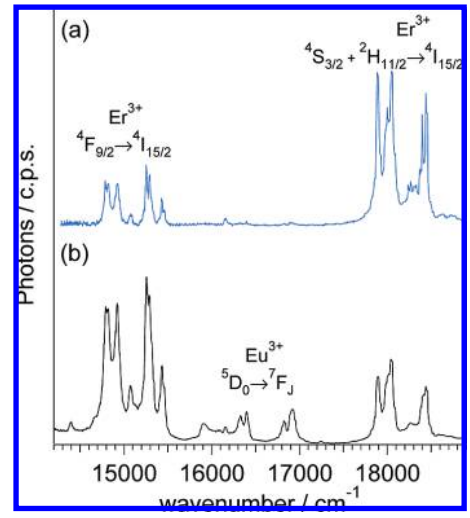

Figure 10. RT UC luminescence spectra exciting at 10 250 cm^{-1} of GGG: 2%Eu^{3+}, 1%Er^{3+} (a) and GGG: 2%Eu^{3+} 5%Yb^{3+} (b).

around 15 000 and 18 000 cm^{-1}, assigned to the Er^{3+} $^4F_{9/2} \rightarrow {}^4I_{15/2}$ and $^4S_{3/2} \rightarrow {}^4I_{15/2}$ transitions, respectively, with the absence of Eu^{3+} emission. We can conclude that excitation at 10 250 cm^{-1} induces Er^{3+} luminescence but it is not able to induce Eu^{3+} luminescence. Therefore, we exclude any relevant role of Er^{3+} in the Yb^{3+} to Eu^{3+} UC luminescence.

iii. UC Mechanism. Tb^{3+} and Eu^{3+} UC luminescence is obtained upon excitation at 10 250 cm^{-1} in the $^2F_{5/2}$ level of Yb^{3+}. The Tb^{3+} and Eu^{3+} ions have no excited states resonant with the Yb^{3+} transition $^2F_{7/2} \rightarrow {}^2F_{5/2}$ in the IR region, therefore the UC emission cannot be explained by a direct transfer from the excited Yb^{3+} to a Tb^{3+} or Eu^{3+} ion. A cooperative GSA/ESA mechanism in $Yb^{3+}-Tb^{3+}$ dimers coupled by exchange was demonstrated to be responsible of UC Tb^{3+} emission after Yb^{3+} excitation in $Cs_3Tb_2Br_9$: Yb^{3+} at low temperatures.[22] However, the crystal structures of the title compounds are not able to accommodate $Tb^{3+}-Yb^{3+}$ ($Eu^{3+}-Yb^{3+}$) dimers. Therefore, GSA/ESA can be ruled out as a mechanism responsible for the UC luminescence. Additionally, UC phenomena in $Tb^{3+}-Yb^{3+}$ ($Eu^{3+}-Yb^{3+}$) systems have been explained as a cooperative sensitization.[8] Strek et al. proposed two mechanisms to explain the anti-Stokes emission of $KEu_{0.2}Yb_{0.8}(WO_4)_2$ following the Yb^{3+} excitation, which are cooperative sensitization and a process based on Yb^{3+} pairs.[11] The unambiguous manner to investigate the mechanism involved in the UC luminescence is to study its temporal evolution under pulsed excitation.[22] The cooperative sensitization, a three ions process, involves energy transfer from two sensitizers (Yb^{3+} ions) to the activator (Tb^{3+} or Eu^{3+}). This is a slow process that can be

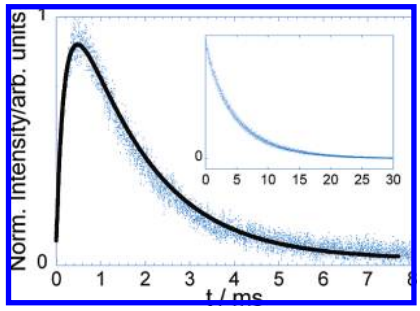

Figure 11. Temporal evolution of Tb^{3+} $^5D_4 \rightarrow {}^7F_J$ UC emission intensity in YAG:2%Tb^{3+}, 5%Yb^{3+} detecting at 18 396 cm^{-1} after pulsed excitation at 10 300 cm^{-1}. The inset shows the lifetime of Tb^{3+} $^5D_4 \rightarrow {}^7F_J$ luminescence upon direct excitation at 20 365 cm^{-1}.

TABLE I: Lifetimes of the $^5D_4$ of Tb^{3+} and $^5D_0$ of Eu^{3+} Levels in Different GGG and YAG Samples Measured after Direct Excitation at the Emission Energy, E_{em}

sample	E_{em}/cm^{-1}	τ/ms
GGG:2%Tb^{3+}, 5%Yb^{3+}	18 396	4.2
YAG:2%Tb^{3+}, 5%Yb^{3+}	18 396	4.9
GGG:2%Eu^{3+}, 5%Yb^{3+}	14 134	4.0
YAG:2%Eu^{3+}, 5%Yb^{3+}	14 090	4.6

active during the Yb^{3+} lifetime (see below). The time evolution of the $^5D_4 \rightarrow {}^7F_J$ Tb^{3+} and $^5D_0 \rightarrow {}^7F_J$ Eu^{3+} luminescence was recorded after direct excitation at around 20 365 and 16 920 cm^{-1} for Tb^{3+} and Eu^{3+}, respectively. Experimental data have been fitted to a single exponential (see inset on Figure 11); the corresponding lifetimes are shown in Table I. It is worth to mention that the obtained lifetimes for the Tb^{3+} and Eu^{3+} ions in nanocrystalline GGG and YAG are significantly longer than the usual values found for the doped bulk oxide counterparts.[23] This behavior was also observed for nanocrystalline Eu^{3+}-doped Y_2O_3[24] and ZrO_2[25] powders and it is compatible with the small particle size (size range around 40 nm) and the porous nature (see TEM images, Figure 3) of the nanopowders. In fact, the lengthening of the lifetimes are due to a lower refractive index (n_{eff}) surrounding the lanthanide ions in the nanocrystalline material with respect to the micrometer or submicrometer size host and therefore the filling factor (the fraction of the volume of the host occupied by the nanoparticles) is lower than one.[26]

A lifetime of 490 μs was obtained for the $^2F_{5/2} \rightarrow {}^2F_{7/2}$ Yb^{3+} luminescence in YAG: 2%Tb^{3+}, 5%Yb^{3+}. The temporal evolution of the $^5D_4 \rightarrow {}^7F_J$ Tb^{3+} luminescence obtained after Yb^{3+} excitation at 10250 cm^{-1} for the YAG: 2%Tb^{3+}, 5%Yb^{3+} sample is shown in Figure 11. The rise of the luminescence intensity after IR excitation is a clear fingerprint of an energy transfer process.

The mechanism responsible of Tb^{3+} and Eu^{3+} UC luminescence in GGG and YAG systems codoped with Yb^{3+} involve three ions and it is depicted in Figures 5 and 9. We propose the cooperative sensitization as the mechanism responsible for the Tb^{3+} and Eu^{3+} UC luminescence: two Yb^{3+} ions in the excited state transfer nonradiatively the energy to the $^5D_4$ or $^5D_2$ states of Tb^{3+} or Eu^{3+}, respectively.

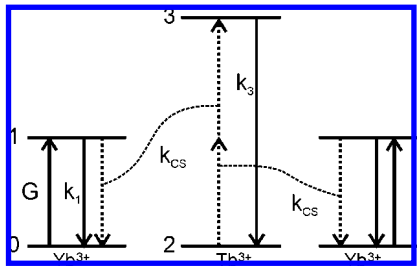

Figure 12. Diagram of the cooperative sensitization of Tb^{3+} or Eu^{3+} luminescence. In this process two excited Yb^{3+} ions transfer nonradiatively their energy to Tb^{3+} or Eu^{3+} ions.

The temporal evolution in Tb−Yb and Eu−Yb systems can be simulated by considering a cooperative sensitization mechanism. Taking into account a four levels system schematically shown in Figure 12, we can write down the four coupled differential rate equations describing the populations of each level, N_i

$$\frac{dN_0}{dt} = -GN_0 + \frac{N_1}{\tau_1} + 2k_{CS}N_1^2N_2$$

$$\frac{dN_1}{dt} = GN_0 - \frac{N_1}{\tau_1} - 2k_{CS}N_1^2N_2$$

$$\frac{dN_2}{dt} = \frac{N_3}{\tau_3} - k_{CS}N_1^2N_2$$

$$\frac{dN_3}{dt} = -\frac{N_3}{\tau_3} + k_{CS}N_1^2N_2$$

where τ_1 and τ_3 represent the Yb^{3+} $^2F_{5/2}$ and Tb^{3+} (Eu^{3+}) $^5D_4$ ($^5D_0$) lifetimes, respectively, G is the power dependence GSA rate constant and k_{CS} is the cooperative sensitization rate parameter. N_0 and N_2 are known from Yb^{3+} and Tb^{3+} concentration values, respectively, whereas N_1 and N_3 are an initial hypothesis since they cannot be experimentally measured. Values of 500 ± 10 μs and 1.8 ± 0.1 ms were obtained from independent measurements for τ_1 and τ_3, respectively. It is possible to obtain the only unknown parameter, k_{CS}, by fitting the time dependent evolution of the UC luminescence, obtained experimentally after short-pulsed excitation into the Yb^{3+} $^2F_{5/2}$ level, to this set of equations. In this way, a value of 1350 s^{-1} was determined for the energy transfer rate constant, $k_{CS}N_1N_2$. The physical meaning of this set of equation is the following; The rise is related with half of the Yb^{3+} $^2F_{5/2}$ lifetime, that would correspond to the lifetime of Yb^{3+} pairs, whereas the decay is related to the Tb^{3+} (Eu^{3+}) $^5D_4$ ($^5D_0$) lifetime. The Tb^{3+} lifetime observed in the UC decay transients was a little bit shorter than that obtained after direct excitation (See Figure 11). This difference is related to the fact that not all Tb^{3+} have necessarily an Yb^{3+} pair as a close neighbor. In UC measurements only those Tb^{3+} which are close to Yb^{3+} ions are excited, whereas after direct excitation all Tb^{3+} are involved.[27]

4. Conclusions

In this paper GGG and YAG nanoparticles doped with Yb^{3+} and Tb^{3+} or Eu^{3+} have been prepared by a sol gel Pechini method. The average size of the particles are 30−40 nm, as shown by TEM measurements. We have studied and identified Tb^{3+} and Eu^{3+} luminescence. Excitation in the NIR region around 10 250 cm^{-1} leads to strong visible Tb^{3+} and Eu^{3+} UC emission at RT. The experimental results and theoretical rate equations model confirm the cooperative sensitization UC mechanism as responsible of the visible UC luminescence. The presence of Er^{3+} and its consequent luminescence upon 10 250

cm^{-1} excitation in $Eu^{3+}-Yb^{3+}$ codoped systems is not relevant for the $Eu^{3+}-Yb^{3+}$ UC mechanism.

Acknowledgment. This work was financially supported by the Spanish Ministerio de Educación y Ciencia under Project No. MAT2005-00099. The authors are grateful to J. Fernández, R. Balda, and S. García-Revilla for their help with Yb^{3+} lifetime measurements.

References and Notes

(1) Joubert, M. F. *Opt. Mater.* **1999**, *11*, 181.
(2) Sivakumar, S.; Diamente, P. R.; van Veggel, F. C.; J, M. *Chem.—Eur. J.* **2002**, *12*, 5878.
(3) Meiser, F.; Cortez, C.; Caruso, F. *Angew. Chem., Int. Ed.* **2004**, *43*, 5954.
(4) Trupke, T.; Shalav, A.; Richards, B. S.; Würfel, P.; Green, M. A. *Solar Energy Mater. Solar Cells* **2006**, *90*, 3327.
(5) Nyk, M.; Kumar, R.; Ohulchanskyy, T. Y.; Bergey, E. J.; Prasad, P. N. *Nano Lett.* **2008**, *8* (11), 3834.
(6) Heer, S.; Kömpe, K.; Güdel, H. U.; Haase, M. *Adv. Mater.* **2004**, *16*, 2102.
(7) Boyer, J. C.; Vetrone, F.; Capobianco, J. A.; Speghini, A.; Bettinelli, M. *Chem. Phys. Lett.* **2004**, *390*, 403.
(8) Ostermayer, F. W.; van Uitert, L. G. *Phys. Rev. B* **1970**, *1*, 4208.
(9) Vergeer, P.; Vlugt, T. J. H.; Kox, M. H. F.; den Hertog, M. I.; van der Eerden, J. P. J. M.; Meijerink, A. *Phys. Rev. B* **2005**, *71*, 014119.
(10) Maciel, G. S.; Biswas, A.; Prasad, P. N. *Opt. Commun.* **2000**, *178*, 65.
(11) Strek, W.; Deren, P. J.; Bednarkiewicz, A.; Kalisky, Y.; Boulanger, P. *J. Alloys Compounds* **2000**, *300−301*, 180.
(12) Boyer, J. C.; Vetrone, F.; Capobianco, J. A.; Speghini, A.; Zambelli, M.; Bettinelli, M. *J. Lumin.* **2004**, *106*, 263.
(13) Pechini, M. P. U.S. Patent 3,330,697, 1967.
(14) Daldosso, M.; Falcomer, D.; Speghini, A.; Ghigna, P.; Bettinelli, M. *Opt. Mat.* **2008**, *30*, 1162.
(15) Luterotti, L.; Gialanella, S. *Acta Mater.* **1998**, *46*, 101.
(16) Daldosso, M.; Falcomer, D.; Speghini, A.; Bettinelli, M.; Enzo, S.; Lasio, B.; Polizzi, S. *J. Alloys Compounds* **2008**, *451*, 553.
(17) Blasse, G.; Bril, A. *Philips Res. Repts.* **1967**, *22*, 481.
(18) Dorenbos, P. *J. Lumin.* **2000**, *91*, 91.
(19) Sivakumar, S.; van Veggel, F. C. J. M. *J. Disp. Technol.* **2007**, *3* (2), 176.
(20) Van der Weg, W. F.; Popma, Th. J. A.; Vink, A. T. *J. Appl. Phys.* **1985**, *57*, 5450.
(21) Wang, H.; Duan, C.; Tanner, P. A. *J. Phys. Chem. C* **2008**, *112*, 16651.
(22) Salley, G. M.; Valiente, R.; Güdel, H. U. *Phys. Rev. B* **2003**, *67*, 134111.
(23) X. Liu, X.; Wang, X.; Wang, Z. *Phys. Rev. B* **1989**, *39* (15), 10633.
(24) Meltzer, S.; Feofilov, S. P.; Tissue, B.; Yuan, H. B. *Phys. Rev. B* **1999**, *60*, R14012.
(25) Speghini, A.; Bettinelli, M.; Riello, P.; Bucella, S.; Benedetti, A. *J. Mater. Res.* **2005**, *20*, 2780.
(26) Hreniak, D.; Strek, W.; Gluchowski, P.; Bettinelli, M.; Speghini, A. *Appl. Phys. B: Laser Opt.* **2008**, *91*, 89.
(27) Salley, G. M.; Valiente, R.; Güdel, H. U. *J. Phys.: Condens. Matter* **2002**, *14*, 5461.

JP901711G